Journal of Rock Mechanics and Geotechnical Engineering 11 (2019) 1201–1210

Contents lists available at ScienceDirect

Journal of Rock Mechanics and Geotechnical Engineering

journal homepage: www.rockgeotech.org

Full Length Article

Numerical study of the circular opening effect on mechanical behaviour of rock under confinement

Y.L. Gui [a], J.L. Shang [b,*], J.J. Ma [c], Z.Y. Zhao [b]

[a] School of Engineering, Newcastle University, Newcastle upon Tyne, NE1 7RU, United Kingdom
[b] School of Civil and Environmental Engineering, Nanyang Technological University, 639798, Singapore
[c] School of Civil Engineering, Sun Yat-Sen University, Guangzhou, 510275, China

ARTICLE INFO

Article history:
Received 31 August 2018
Received in revised form
25 February 2019
Accepted 7 March 2019
Available online 1 August 2019

Keywords:
Rock with opening
Simulation
Biaxial loading
Strength
Stiffness

ABSTRACT

Opening holes in rock including their size and distribution can affect the performance of rock-related structures. A good understanding on this will contribute to, for example, rock cavern design, and construction, tunnelling, and mining engineering. To improve the understanding, a comprehensive investigation of the opening hole effect on the rock mechanical behaviour under biaxial loading condition is carried out by virtue of a hybrid continuum-discrete element method. Laboratory specimens with both single hole and multi-hole of various radii are investigated and compared with the cases subjected to uniaxial compression. It is demonstrated that the confining pressure can increase both the stiffness and strength due to delaying the crack initiation and propagation. The increase due to the confining pressure is more evident for the compressive strength. For single hole specimens with 0.75 mm radius hole, the increase ratio of the compressive strength is a linear increasing function with width and the increase ratio ranges from 2.15 for the specimen with 3.5 mm width to 2.45 for 10 mm width. For the single hole specimen with 10 mm width, the increase ratio starts at 2.13 for the specimen with 0.75 mm radius hole, ascending to the peak of 2.37 for the specimen with 1 mm radius hole, followed by a decline to 2.2 for the specimen with 1.25 mm radius hole. However, for the multi-hole specimens, the increase ratio varies from 1.66 to 3.13. In addition, to verify the influence of confining pressure magnitude on the performance of the rock specimens, totalling 10 confining pressure levels are applied and modelled. The simulation results show that even though there are opening holes in the specimens, the simulated compressive strength generally follows the generalised Hoek-Brown model.

1. Introduction

Rock is non-homogeneous material and normally contains various defects, for example, beddings, faults, and opening cavities. These defects influence the strength and stiffness of rock significantly. When subjected to internal and external loadings, they can propagate, interact and sometimes coalescence, resulting in damage or failure (Gui et al., 2017). The rock with opening holes therefore has received wide attentions in rock engineering related to rock excavation, for instance, civil and mining engineering. A number of studies have been conducted on the failure mechanism of artificially flawed rock/rock-like materials for mimicking intact rock. The available approaches include laboratory testing (e.g. Bobet and Einstein, 1998; Wong et al., 2006; Haeri et al., 2014; Yang et al., 2015a), numerical simulation (e.g. Gui et al., 2017; Peng et al., 2018), and analytical modelling (e.g. Sammis and Ashby, 1986; Masoudian and Hashemi, 2016; Masoudian et al., 2018; various others summarised by Jaeger et al., 2007). However, there is limitation in laboratory testing or theoretical analysis. For example, (a) mineral effect (i.e. content and spatial distribution) is inevitable in laboratory testing, due to the geological process during formation of the rock; and (b) the stress–strain analysis from analytical simulation can only be possible for simple alignments of opening holes, for example, single centre-located hole with given far-field principal stresses (Jaeger et al., 2007). Numerical simulation can be more effective as identical model with more complex opening alignments can be easily handled. In the literature, the numerical methods used are primarily based on finite element method (FEM), finite difference method (FDM), discrete element method (DEM)

* Corresponding author.
E-mail address: shangjunlongcsu@gmail.com (J.L. Shang).
Peer review under responsibility of Institute of Rock and Soil Mechanics, Chinese Academy of Sciences.

https://doi.org/10.1016/j.jrmge.2019.07.003

(Gui et al., 2013; Gui and Zhao, 2015; Choo et al., 2016), and hybrid method (Gui et al., 2017). A comprehensive literature review on numerical methods applied on rock cracking simulation has been carried out in Gui et al. (2016a) that the interested readers are encouraged for more information.

The main contribution carried out in the literature has been the studies of rock fracturing under uniaxial loading condition for fissured rock (Yang et al., 2014, 2015b). The study of rock with opening holes has not been fully understood in the literature yet. However, the problem of circular holes in rock is of critical importance as most holes drilled through rock are circular cross-section (Jaeger et al., 2007). This is the scenario that circular opening is chosen in this work. In addition, a loading scenario closer to the in situ rock loading condition should be carried out in order to investigate rock behaviour under in situ stress condition.

The paper aims to investigate the influence of the opening hole on rock's strength, stiffness and crack initiation and propagation under biaxial loading condition. The mechanical behaviour of the rock is investigated based on the distribution of the principal stresses in the rock specimens. The aspects that the paper covers include: (i) the single circular hole effect on the mechanical behaviour for rock; (ii) the multiple circular hole effect on the mechanical behaviour for rock; (iii) the principal stress inside rock specimen; and (iv) the effect of confinement on the mechanical behaviour for rock with multi-hole (this is not covered in the literature). The simulation results demonstrate that the opening including its size and alignment in rock can significantly change the rock mechanical behaviour in terms of strength and stiffness deterioration as well as cracking behaviour under biaxial confinement.

2. Numerical method

The numerical method used in this paper is UDEC, which is a hybrid continuum-discrete element method (Itasca, 2008; Gui et al., 2015, 2016a, b, 2017). The method can capture the interaction of discrete granular materials because of its DEM nature, and the solid continuum within discrete bodies due to its continuum-mechanics theory used in the method. It can also model the fracturing process in materials. Similar to classical DEM-like particle flow code (PFC) (Potyondy and Cundall, 2004), in this method, the material is represented by an assemblage of discrete grains (representing rock blocks) which are internally meshed to model their own continuum mechanical behaviour. The cracks or potential cracks in the materials are represented by the bond between the grains (Fig. 1). The bond is comprised of several pairs of contacts depending on the mesh refinement inside the grains. In this method, the contacts are elastic and governed by Coulomb-slip model (Itasca, 2008) and the grains themselves in the hybrid method are represented as elastic. The forces and displacements across these contacts and the grains' motion are updated step by step during calculation. In this model, Voronoi grains are used to simulate the potential fracturing path for the rock under compression. Using Voronoi grains is not the purpose of simulating any particular geological fracture pattern observed in rock mass in field. In other words, using Voronoi grains in this numerical model is in fact to minimise mesh bias so that artificially predetermined fracturing path can be avoided by letting the model itself to determine. If a particular field fracture pattern is of interest, another set of joints representing the field fracture is needed in order to understand its influence. In the simulations, due to the original shape of the rock specimens (rock brick), plane-strain condition is used for all specimens as the strain along the orientation perpendicular to the plane is negligible.

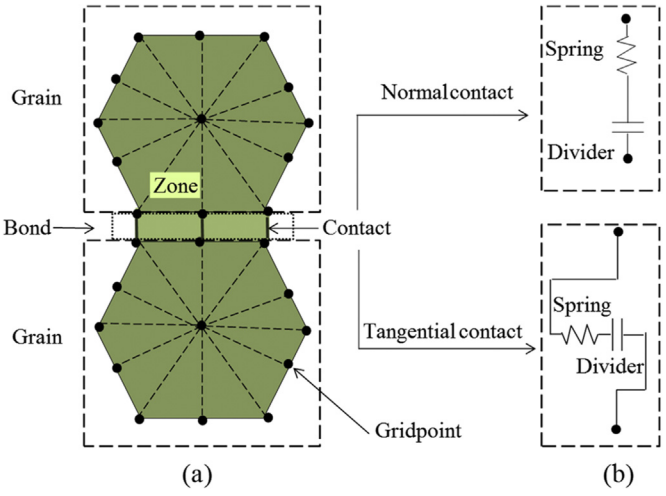

Fig. 1. Sketch of the hybrid numerical method and its contact model (Gui et al., 2017).

3. Simulation results

Table 1 lists the parameters applied in the numerical simulations, which are based on the calibration of the laboratory uniaxial compression tests by Wong et al. (2006) on Hong Kong granite. More information about the model calibration and verification can be found in Gui et al. (2017). It is worth noting that the numerical modelling is for the laboratory scale and it is not the full-scale for tunnels. However, considering the nature of the numerical method, the simulation results can be used to suggest the influence of the opening hole on the stiffness and strength of the rock mass, for example, tunnelling. The numerical models for the specimens discussed in the paper are presented in Fig. 2.

3.1. Specimen width effect

The specimens with single hole used in this study are shown in Fig. 2a. The height of the single hole specimens is 24 mm, while their width varies with value of 3.5 mm, 7 mm, 10 mm, 10 mm and 10 mm, respectively. The radius of the centre holes is 0.75 mm, 0.75 mm, 0.75 mm, 1 mm and 1.25 mm, respectively. The grain effect in the numerical method has been discussed in the work by Gui et al. (2016b). Confinement of 5 MPa is applied on both left and right boundaries of each specimen.

Table 2 presents the simulated Young's modulus and compressive strength. It can be seen that for the specimens with hole size of 0.75 mm, the simulated Young's modulus and compressive strength are both increased with the increase of the specimens' width. Specifically, for Young's modulus, it is raised from 31.44 GPa (with 3.5 mm width) to 33.84 GPa (with 10 mm width). The compressive strength increases from 158.39 MPa for specimen with width of 3.5 mm to 264.23 MPa for that with width of 10 mm. One of the reasons is that the specimen's cross-sectional area is actually dependent on its width, and larger width induces larger cross-

Table 1
Parameters used in the numerical simulations (Gui et al., 2017).

ρ (kg/m^3)	E (GPa)	ν	k_n (Pa/m)	k_s (Pa/m)	σ_t (MPa)	c (MPa)	φ (°)
2601	80	0.34	8×10^{13}	4×10^{13}	10	20	40

Note: ρ - density; E - Young's modulus; ν - Poisson's ratio; k_n - normal stiffness; k_s - shear stiffness; σ_t - tensile strength; c - cohesion; φ - friction angle.

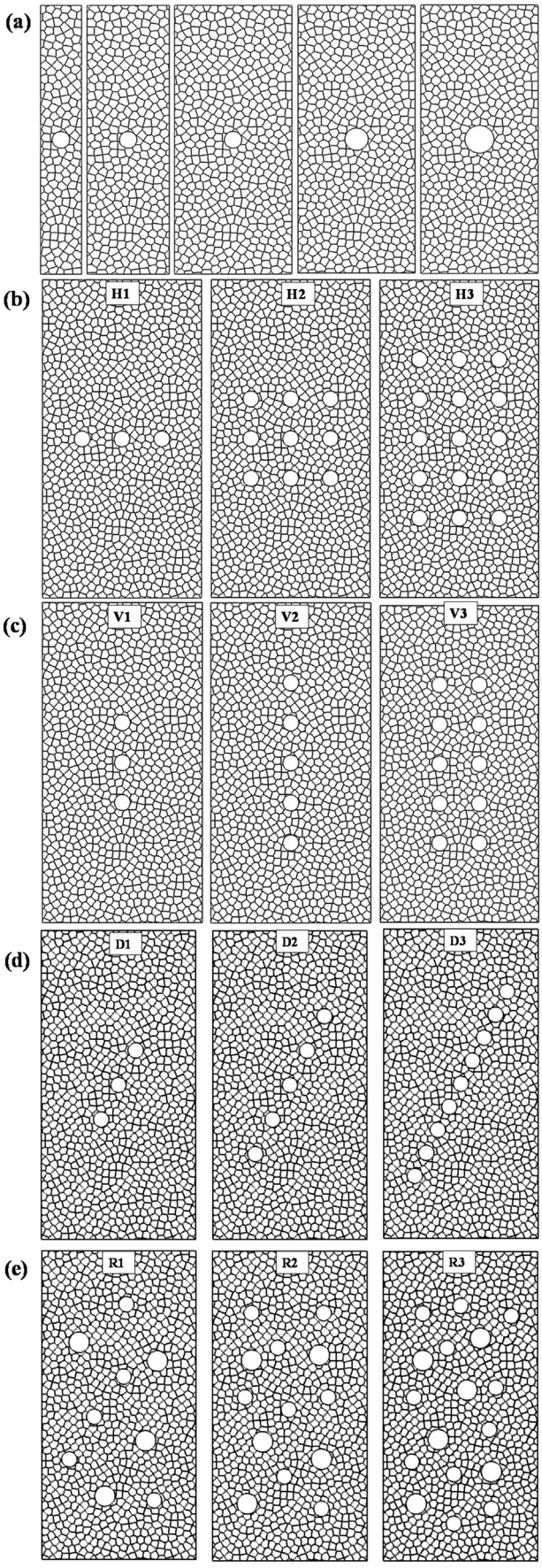

Fig. 2. Established numerical models used in the simulations (Gui et al., 2017).

sectional area. Therefore, if increases the width, the compressive strength and Young's modulus will be ascended. The results of uniaxial compression simulations are also presented in Table 2 as a comparison to demonstrate the significance of confinement on the performance of rock in terms of stiffness and strength increment. It is found that the confinement of 5 MPa can increase the compressive strength significantly – more than 2 times of that without confinement. Nevertheless, the influence on Young's modulus is nearly negligible as demonstrated in Table 2.

The compressive stress–strain relationships for the five specimens under uniaxial and biaxial compression conditions are presented in Fig. 3. It is shown that under biaxial compression condition, the stress–strain relationship has more inelasticity before the peak stress due to the lateral confinement. The post-peak behaviour of the specimen with the smallest width shows the largest ductility under confinement compared to the other four specimens.

Fig. 4a plots the relationships among the compressive strength under biaxial and uniaxial loadings, compressive strength increase ratio, and the normalised specimen width, for the three specimens with the same hole size but different widths. It conveys that the compressive strength obtained from both biaxial and uniaxial loading cases is monotonically decreasing function of normalised specimen width. Nevertheless, the compressive strength increase ratio is not a monotonic function of the normalised specimen width; rather, the confinement has the greatest influence on the compressive strength increment for the rock specimen with a width of 7 mm among the three specimens. The increase ratio is generally over 2 for the three specimens (Table 2).

To understand the mechanism of the observations, the principal stresses inside the specimens are investigated, as shown in Fig. 5. The microcrack patterns inside the specimen experiencing the same vertical strain (i.e. 9.55×10^{-4}) are also demonstrated in Fig. 5. It is observed that the main part of the specimens is under compression for the major and minor principal stresses. Nonetheless, the major principal stress is tensile at the top and bottom of the centre hole, while the left and right wings of the hole are overall under compression, especially for Fig. 5a and b under uniaxial loading. However, it reasonably assumes that Fig. 5c and all the specimens under biaxial compression would experience similar major principal stress distribution if the vertical compressive strain had been increased to a higher level. The minor principal stress shows an 'X' shape in which the stress is under tension; while the top, bottom, left and right wings of the hole are generally under compression. This is obvious in biaxial compression simulations. It is worth noting that the slim specimen (Fig. 5a) has been affected by the lateral confining pressure more significantly than the wider specimens (Fig. 5b and c).

Due to the confining pressure in biaxial compression simulations, the tensile zone length is shorter than that in uniaxial compression simulations with smaller tensile stress. Comparing the three specimens, it is found that the tensile zone length is prohibited if increasing the specimen width so that shorter cracks at the top and bottom wings of the opening hole under the same axial strain are induced. The microcracks at the top and bottom of the hole are governed by the tension of the major principal stress. Due to the confinement, the crack initiation and propagation have been postponed in the biaxial compression simulations. Eventually, the postponement results in a higher compressive strength in biaxial compression simulations, as presented in Fig. 3b and Table 2.

3.2. Hole size effect

In this section, the hole size effect on the specimens with identical width is discussed. It can be seen in Table 2 that the

Table 2
Simulation results for single hole specimen.

H (mm)	W (mm)	R (mm)	E (GPa)		σ_c (MPa)		Increase ratio of σ_c
			U	B	U	B	
24	3.5	0.75	28.65	31.44	71.87	158.39	2.2
24	7	0.75	31.15	33.5	108.66	257.13	2.37
24	10	0.75	31.54	33.84	124.01	264.23	2.13
24	10	1	30.97	33.26	112.15	257.11	2.29
24	10	1.25	30.52	32.59	91.46	224.12	2.45

Note: H - height; W - width; R - hole radius; σ_c - compressive strength; U and B - uniaxial and biaxial compression (with confining pressure of 5 MPa), respectively.

Young's modulus and compressive strength both decrease from 33.84 GPa and 264.23 MPa for specimen with hole radius of 0.75 mm to 32.59 GPa and 224.12 MPa for specimen with hole radius of 1.25 mm, respectively. Similarly, the influence of confinement on the compressive strength is again much more pronounced than that on the Young's modulus. The increase of compressive strength due to the confinement can be found in Fig. 4b and Table 2, suggesting that the influence of lateral pressure has more impact on the specimen with larger hole: the increase ratio is 2.13, 2.29 and 2.45, respectively, for the specimen with hole radius of 0.75 mm, 1 mm and 1.25 mm. The increase ratio is nearly linear with respect to the normalised specimen width.

The principal stress distribution and microcrack pattern at low vertical compressive strain (9.55×10^{-4}) are presented in Fig. 6. Similar to Fig. 5, it is observed that the major principal stress is generally close to zero at the top and bottom wings of the centre hole in all the three specimens and it is much higher than the other areas, while the left and right wings of the hole are overall under compression. However, due to the confining pressure in biaxial compression, the tensile zone length is shorter than that in uniaxial compression, in addition to lower tensile stress. Comparing the three specimens, it is found that the tensile zone length is exaggerated if increasing the hole size, and longer cracks along the top and bottom wings of the hole can be induced under the same vertical strain. Due to the confinement, the crack initiation and propagation have been postponed in biaxial compression. Again, the postponement results in a higher compressive strength in biaxial compression, as presented in Fig. 3b and Table 2.

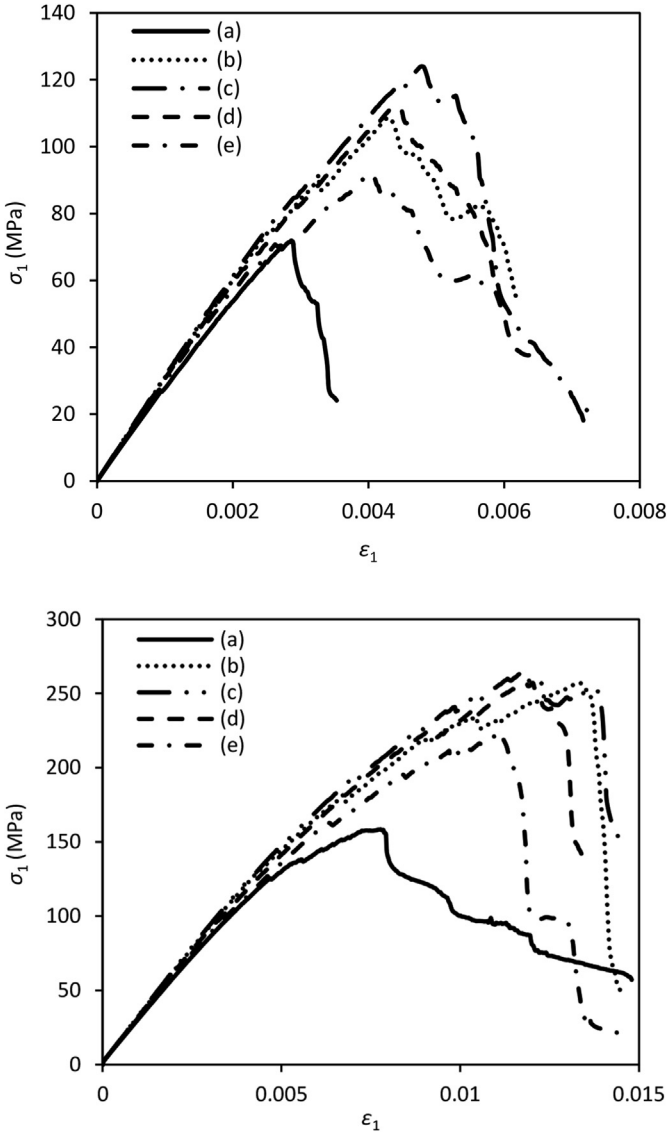

Fig. 3. Modelled axial stress–strain relationships of the specimens. The top figure is the uniaxial compression and the bottom one is the biaxial compression. (a)–(e) correspond to the specimens from the left to the right in Fig. 2a.

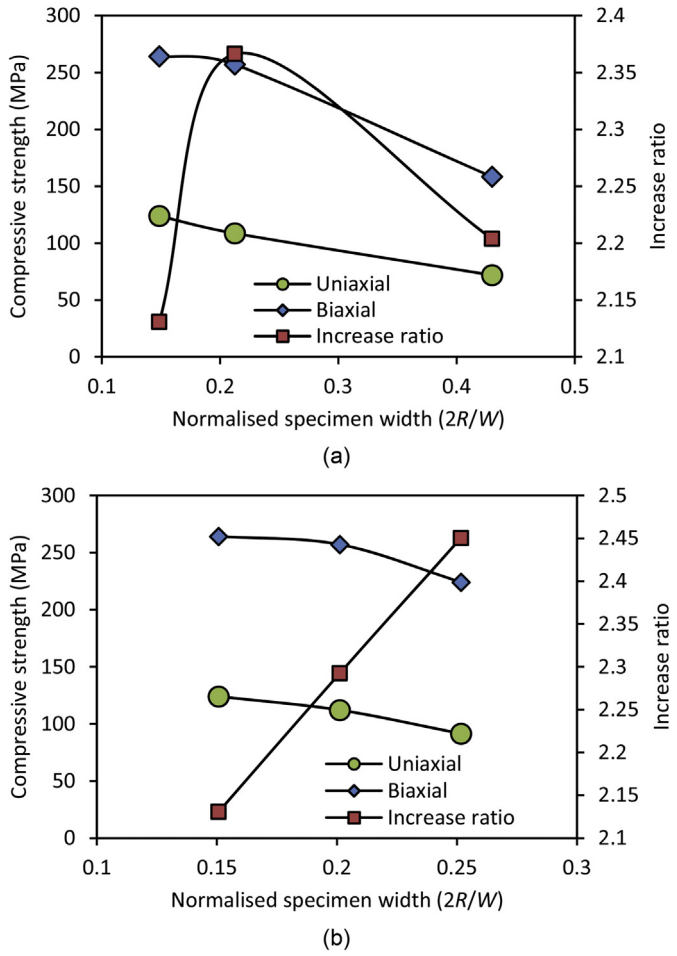

Fig. 4. Relationships between simulated compressive strength and normalised specimen width for (a) the first three specimens in Fig. 2a, and (b) the three specimens in Fig. 2b. The increase ratio is equal to the ratio of biaxial compressive strength to uniaxial compressive strength.

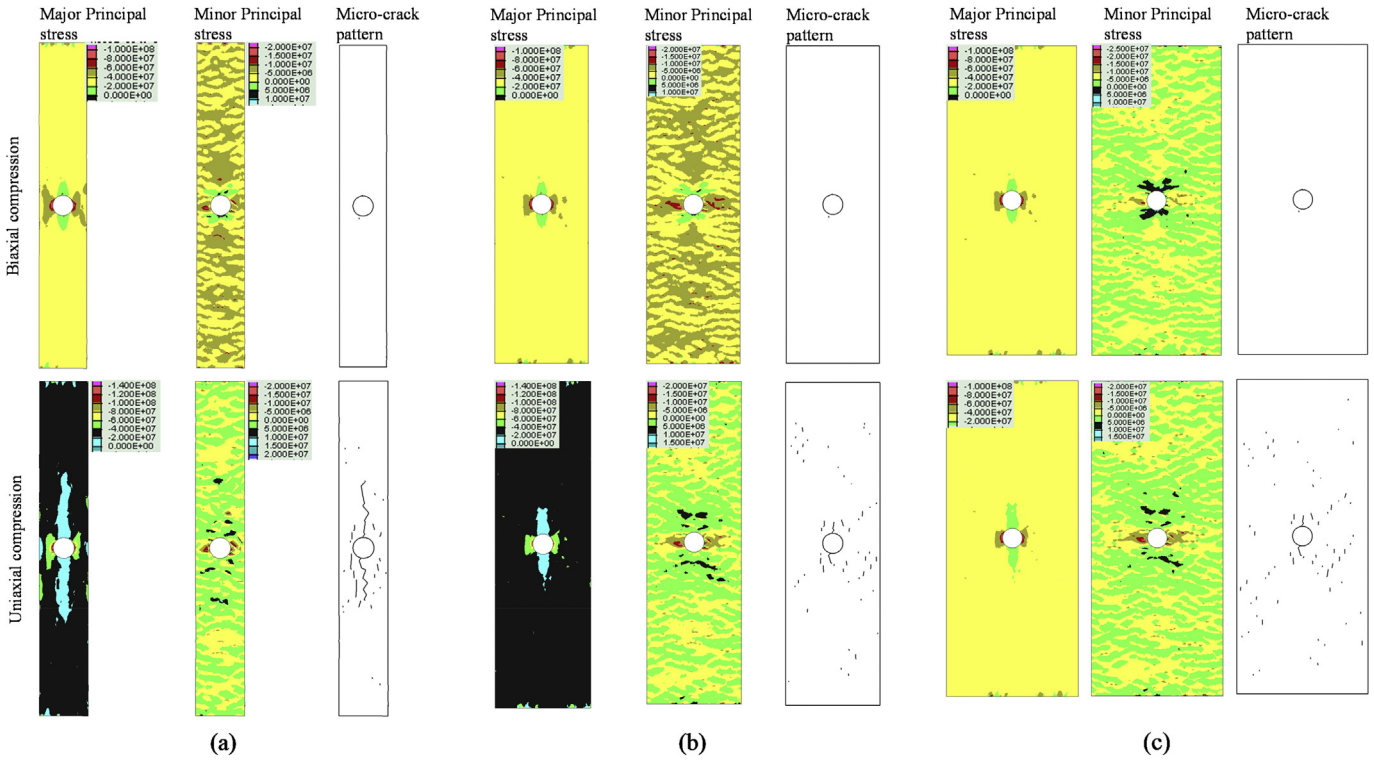

Fig. 5. Principal stresses (Pa) distribution and microcrack pattern for specimens with the same hole size (hole radius of 0.75 mm) under biaxial and uniaxial compression, with vertical strain of 9.55×10^{-4}. The confining pressure for the biaxial compression is 5 MPa. The sample widths are (a) 3.5 mm, (b) 7 mm, and (c) 10 mm. Negative stress represents compression.

3.3. *Hole alignment effect*

In this section, the effect of group of holes on the mechanical behaviour of the rock is presented. It is based on the specimens presented in Lin et al. (2015) (Fig. 2b–e) for Hong Kong granite. The radius of the holes is 0.75 mm. The length of the rock bridge (i.e. distance between two neighbouring holes measured from the hole boundary) is 1.5 times the hole radius, i.e. 1.25 mm. However,

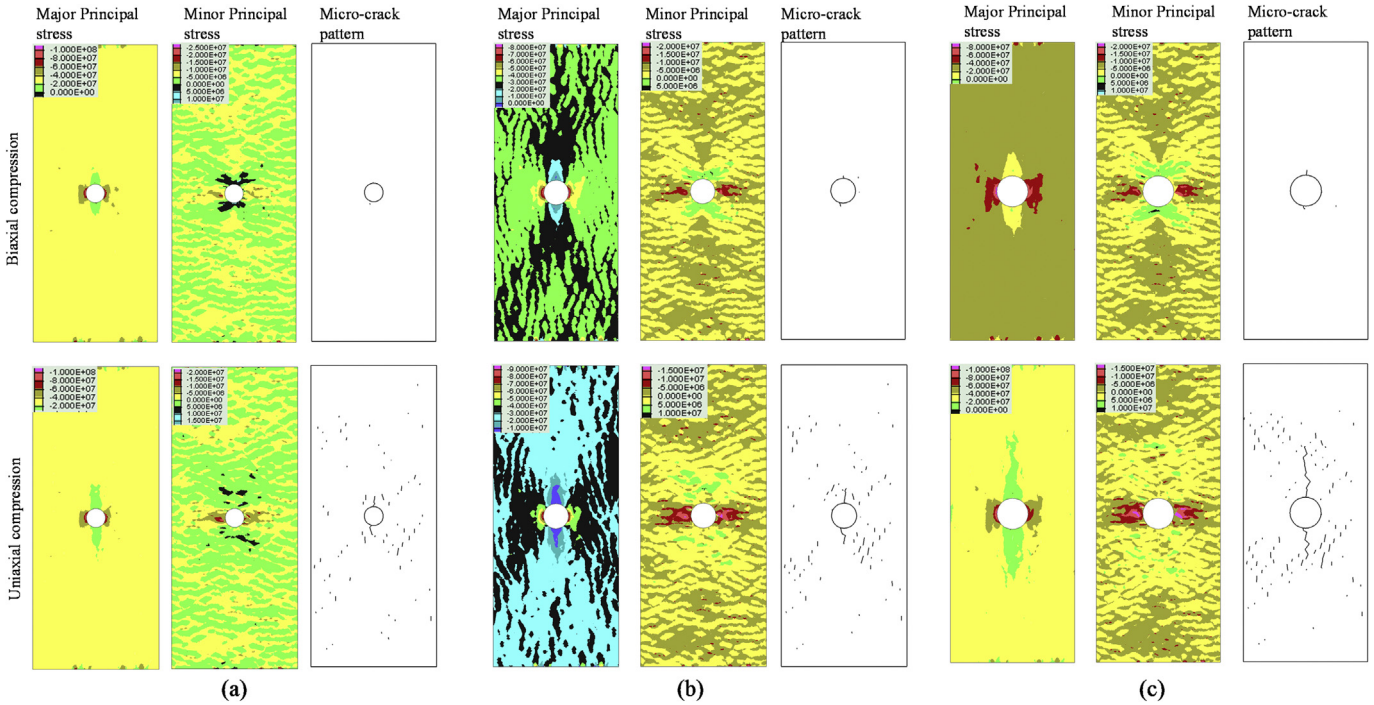

Fig. 6. Principal stresses (Pa) distribution and microcrack pattern for specimens with the same width (10 mm) under biaxial and uniaxial compression, with vertical strain of 9.55×10^{-4}. The confining pressure for the biaxial compression is 5 MPa. The sample hole radii are (a) 0.75 mm, (b) 1 mm, and (c) 1.25 mm. Negative stress represents compression.

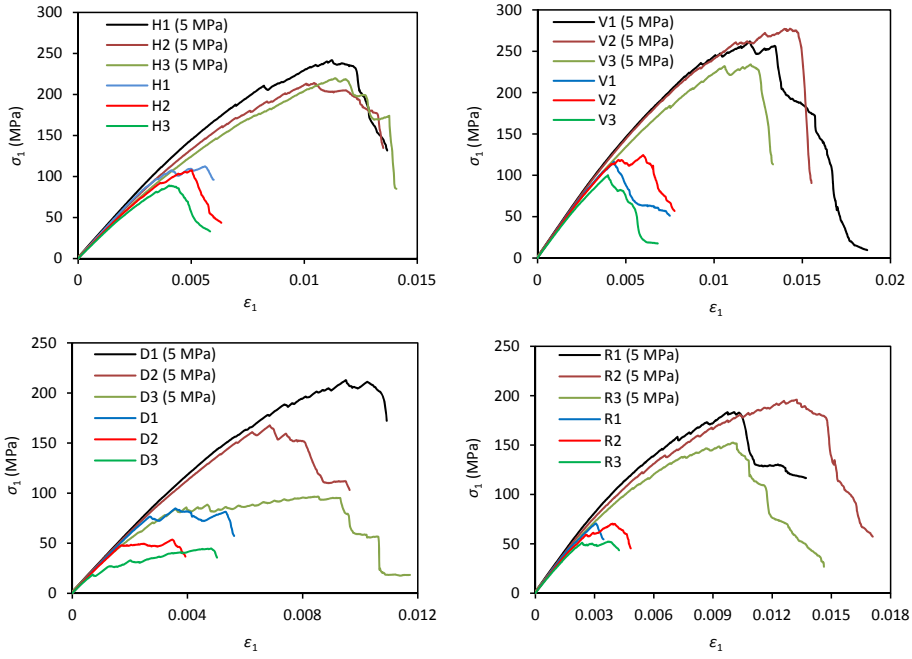

Fig. 7. Compressive stress–strain curves for the specimens with multi-holes under biaxial (confining pressure of 5 MPa) and uniaxial compression.

the bridge length of D3 is only 1 mm due to the specimen's size limitation. The confining pressure for all the specimens with multi-hole is 5 MPa. The modelled stress–strain curves of the samples are presented in Fig. 7. In order to compare the effect of confining pressure on the mechanical behaviour of the rock, the stress–strain curves for the uniaxial compression are also presented in this figure. It can be seen that the slope of the curves before the peak has been slightly increased and the curves reach to a larger peak stress under biaxial loading cases. The simulated values of the compressive strength and Young's modulus are listed in Table 3. It is obvious that the hole alignment has significant impact on the mechanical behaviour of the rock. However, the Young's modulus changes due to the fact that the confining pressure is not as obvious as the compressive strength. The specific increase ratio is also listed in Table 3. The ratio is generally between 2 and 3.

The principal stresses and microcrack pattern under low vertical compressive strain are investigated as presented in Figs. 8–11 for alignments H1, V1, D1 and R1, respectively. In alignment H1 (Fig. 8), the tensile zones of the major principal stress appear at both the top and bottom wings of the holes while the compression zones are observed at the left and right wings of the holes. The confining

Table 3
Summary of the simulation results for multi-hole specimens.

Hole alignment	E (GPa)		σ_c (MPa)		Increase ratio of σ_c
	U	B	U	B	
H1	31.2	31.71	112.28	241.72	2.15
H2	29.35	32.24	107.47	213.88	1.99
H3	27.62	30.57	88.95	219.74	2.47
V1	31.55	31.91	116.31	261.72	2.25
V2	31.04	31.31	124.46	277.3	2.23
V3	29.43	29.83	100	166	1.66
D1	31.19	31.69	84.75	212.84	2.51
D2	30.65	30.75	53.6	167.61	3.13
D3	27.4	27.55	44.76	96.55	2.16
R1	28.14	28.57	70.54	183.36	2.6
R2	26.72	27.16	70.32	195.91	2.79
R3	25.58	25.79	52.27	152.41	2.92

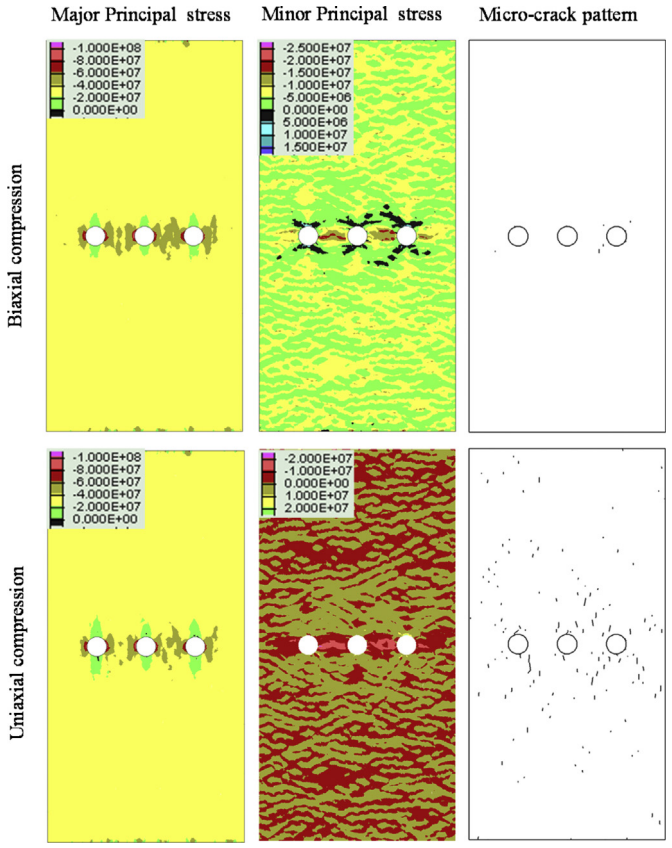

Fig. 8. Principal stresses (Pa) distribution and microcrack pattern for alignment H1 under biaxial and uniaxial compression conditions, with vertical strain of 9.35×10^{-4}. The confining pressure for the biaxial compression is 5 MPa. Negative stress represents compression.

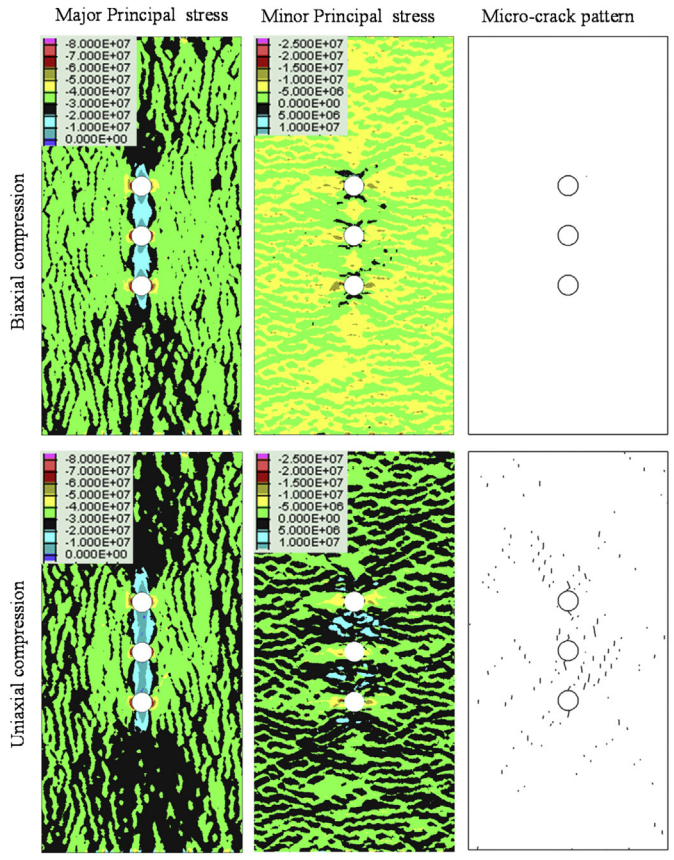

Fig. 9. Principal stresses (Pa) distribution and microcrack pattern for alignment V1 under biaxial and uniaxial compression conditions, with vertical strain of 9.35×10^{-4}. The confining pressure for the biaxial compression is 5 MPa. Negative stress represents compression.

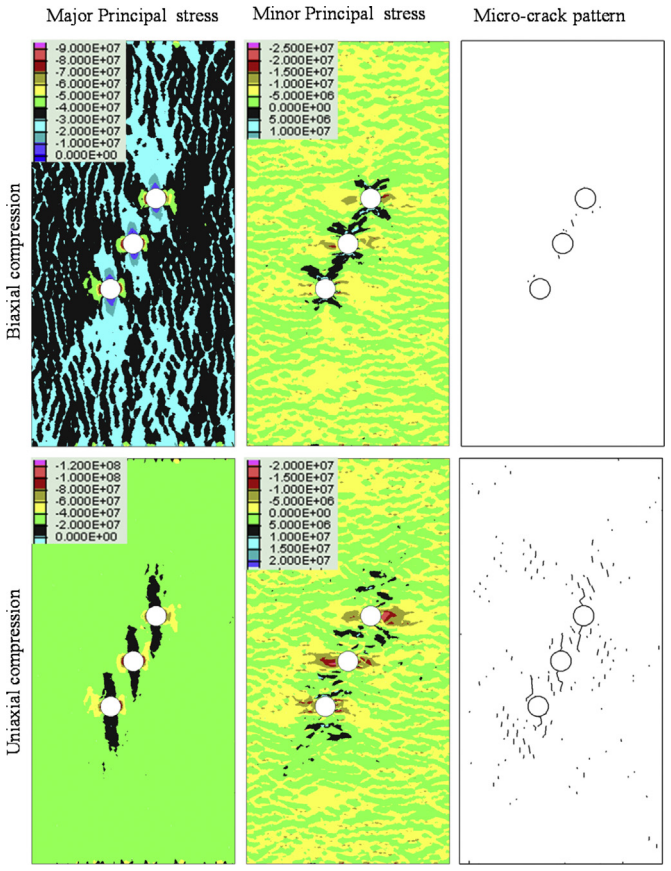

Fig. 10. Principal stresses (Pa) distribution and microcrack pattern for alignment D1 under biaxial and uniaxial compression conditions, with vertical strain of 9.35×10^{-4}. The confining pressure for the biaxial compression is 5 MPa. Negative stress represents compression.

pressure has inhibited the propagation of the tensile zone length of the major principal stress when compared with the uniaxial compression; therefore, the microcrack initiation has been delayed. In terms of the minor principal stress, 'X' shape is observed as similar to the specimens with single hole. However, the compressive minor principal stress between the two adjacent holes is increased (i.e. larger negative values from the contour legend) under both uniaxial and biaxial compression conditions.

In alignment V1 (Fig. 9), the tensile zones of the major principal stress are observed along the three holes and at both top and bottom wings of the holes, while the compression zones are observed at left and right wings of the holes. The confining pressure has inhibited the propagation of the tensile zone length and the magnitude of the major principal stress when compared with uniaxial compression; therefore, the microcrack initiation has been delayed. 'X' shape is observed as similar to the specimens with single hole for the minor principal stress.

For diagonal alignment (e.g. alignment D1) (Fig. 10), at low vertical compressive strain value, the tensile zones of the major principal stress still start from the top and bottom wings of each single hole, while the compressive zones are initiated from the left and right wings. In the minor principal stress distribution, 'X' shape again is observed in two loading scenarios. However, under biaxial compression condition, the top-right wing of the lower holes interacts with the bottom-left wing of the upper holes, as shown in Fig. 10. The microcrack starts earlier in uniaxial compression simulations compared with the microcrack in biaxial compression simulations.

For the random alignment (alignment R1 is used in this paper, Fig. 11), the tensile zones are again observed at the top and bottom of each hole for both loading cases. The left and right of each hole are under compression. The tensile zone length is smaller in biaxial compression simulations due to the confinement; therefore, the microcrack in uniaxial compression initiates prior to that in biaxial compression.

4. Effect of confining pressure

In underground space development, for example, tunnelling, the in situ horizontal stress is more complex compared to the vertical stress. It depends highly on the excavation level/depth, rock properties (e.g. elastic properties, density and thermal expansion coefficient). Brown and Hoek (1978) proposed that the in situ vertical stress (σ_z) follows a linear relationship with depth based on a large number of in situ data. The ratio between the in situ vertical stress and the depth is empirically determined to be 27 MPa/km (Fig. 12a), which is close to the general range of rock unit weight. The ratio (k) between horizontal (σ_h) and vertical (σ_v) in situ stresses was also obtained through a large number of measurement data by Brown and Hoek (1978), as plotted in Fig. 12b.

To further study the influence of various confining pressures on the mechanical behaviour of the rock with holes, nine more confining pressures (i.e. 1 MPa, 2 MPa, 3 MPa, 4 MPa, 6 MPa, 7 MPa, 8 MPa, 9 MPa, and 10 MPa) are applied to the specimens with multiple holes and without hole. It can be seen that the confining pressure investigated here is in good agreement with the practical

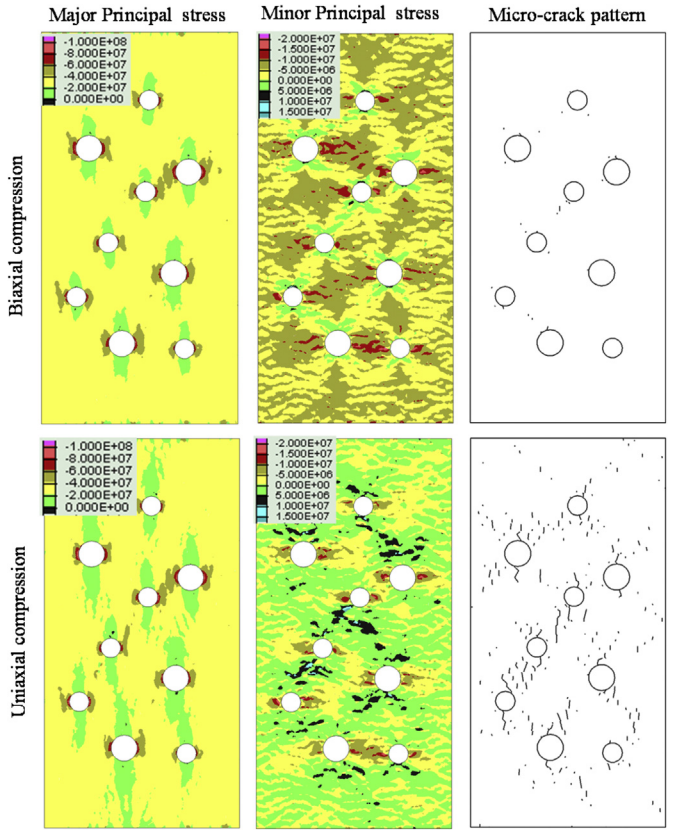

Fig. 11. Principal stresses (Pa) distribution and microcrack pattern for alignment R1 under biaxial and uniaxial compression conditions, with vertical strain of 9.35×10^{-4}. The confining pressure for the biaxial compression is 5 MPa. Negative stress represents compression.

in situ horizontal stress in the ground (Table 4). The corresponding depth of the excavation varies from near ground surface to 1 km depth.

The simulated stress–strain curves are plotted in Fig. 13. It is shown that the change of confining pressure has significant impact on inelastic behaviour before peak. The post-peak ductility is not obvious due to the collapse of the holes under high confining pressure. The influence of confinement is also plotted in Fig. 14 and compared with the fit by Hoek-Brown failure criterion (H–B). The black solid line in Fig. 14 is the fit of H–B model for the specimen without hole. It can be seen that the prediction of H–B model can

Table 4
In situ stresses calculated based on Fig. 12.

Depth (km)	Vertical stress (MPa)	Horizontal stress (MPa)	
		Lower bound	Higher bound
0.001	0.027	2.7081	40.5135
0.01	0.27	2.781	40.635
0.1	2.7	3.51	41.85
1	27	10.8	54
2	54	18.9	67.5

still hold for the range of confining pressure considered. The H–B model used is the generalised form (Hoek et al., 1995):

$$\sigma'_1 = \sigma'_3 + C_0\left(m_b\frac{\sigma'_3}{C_0} + s\right)^a \tag{1}$$

where σ'_1 and σ'_3 are the major and minor principal effective stresses at failure, respectively; m_b is used for broken rock; C_0 is the rock uniaxial compressive strength; and s and a are the dimensionless empirical constants. The parameters m_b, s and a were proposed to be determined by geological strength index (GSI) as follows (Hoek et al., 2002):

$$m_b = m_i \exp\left(\frac{GSI - 100}{28 - 14D}\right) \tag{2}$$

$$s = \exp\left(\frac{GSI - 100}{9 - 3D}\right) \tag{3}$$

$$a = \frac{1}{2} + \frac{1}{6}\left(e^{-\frac{GSI}{15}} + e^{-\frac{20}{3}}\right) \tag{4}$$

where m_i is a curve fitting parameter derived from triaxial testing of intact rock, thus m_b is a reduced value of m_i, accounting for the strength reduction effect of the rock mass conditions by GSI (Marinos et al., 2005; Eberhardt, 2012); and D is the factor used to consider near surface blasting and stress relaxation. The values of parameters used in the generalised H–B model are: $GSI = 91$, $D = 1.79$ and $m_i = 2700$ and they are determined from the best fitting. The uniaxial compressive strength of the rock is 200 MPa obtained by laboratory testing in Wong et al. (2006). To understand the effect of holes on the compressive strength, the specimen without hole is also modelled under the same confining pressures and the simulation result is presented in Fig. 14. Overall, the intact

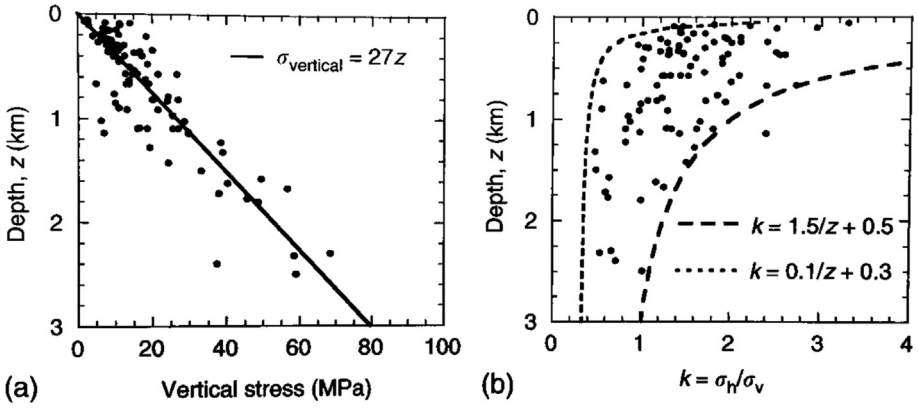

Fig. 12. Measured subsurface data (Brown and Hoek, 1978; Jaeger et al., 2007).

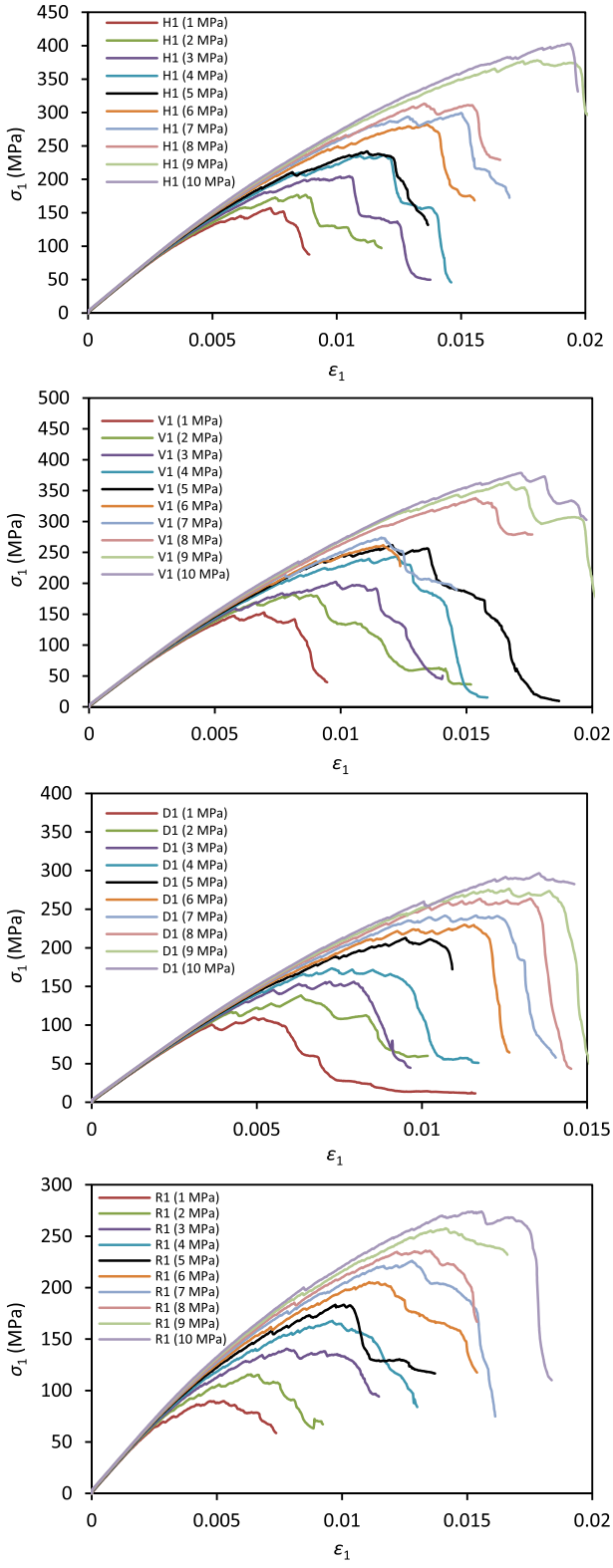

Fig. 13. Effects of various confining pressures on the mechanical behaviour of rock with multiple holes.

rock under each confining pressure shows higher compressive strength than the rock with multi-hole under the same confining pressure. Horizontal and vertical alignments show higher compressive strength than the diagonal and random alignments,

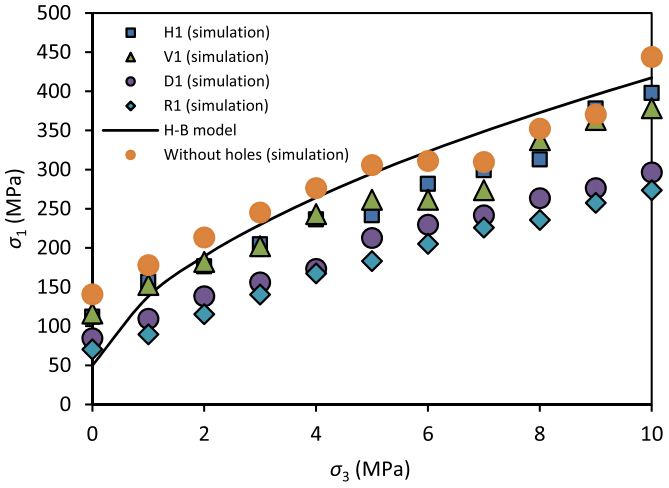

Fig. 14. Effects of confining pressure on intact rock specimen and specimens with multiple holes.

although their opening ratio (i.e. opening area/specimen area) is the same in alignments H1, V1 and D1. The specimen with random alignment shows the lowest compressive strength among the four alignments.

5. Conclusions

A comprehensive study of the influence of opening in rock on its mechanical behaviour including Young's modulus, compressive strength, microcrack propagation as well as the principal stresses distribution in the specimen under biaxial condition has been conducted. Various hole arrangements including single-hole and multi-hole have been considered. It shows that confining pressure can significantly increase compressive strength and slightly increase Young's modulus. For the specimen with single centred-hole, increasing specimen width can increase both Young's modulus and compressive strength. However, increasing hole size in the same sized specimen can decrease the Young's modulus and compressive strength. The impact on the compressive strength is higher for the specimen with larger hole. The mechanism is that the confining pressure could postpone the tensile zone length and its stress level, thereby delaying the microcrack initiation around the hole boundary. For the specimen with multi-hole, the confining pressure has strengthened the specimen, however, with lower strength compared to intact rock. Among the multi-hole specimen, vertical and horizontal alignments have less impact on the strength than the diagonal and random alignments.

Conflicts of interest

We wish to confirm that there are no known conflicts of interest associated with this publication and there has been no significant financial support for this work that could have influenced its outcome.

References

Bobet A, Einstein HH. Fracture coalescence in rock-type materials under uniaxial and biaxial compression. International Journal of Rock Mechanics and Mining Sciences 1998;35(7):863–88.
Brown ET, Hoek E. Trends in relationships between in situ stresses and depth. International Journal of Rock Mechanics and Mining Sciences & Geomechanics Abstracts 1978;15(4):211–25.

Choo LQ, Zhao ZY, Chen HM, Tian Q. Hydraulic fracturing modelling using the discontinuous deformation analysis (DDA) method. Computers and Geotechnics 2016;76:12–22.
Eberhardt E. The Hoek-Brown failure criterion. Rock Mechanics and Rock Engineering 2012;45(6):981–8.
Gui Y, Zhao G, Khalili N. Experimental and numerical modelling of sandstone bending using modified three-point test. In: Rock dynamics and applications - state of the art. London, UK: Taylor and Francis Group; 2013. p. 289–394.
Gui Y, Bui HH, Kodikara J. An application of a cohesive fracture model combining compression, tension and shear in soft rocks. Computers and Geotechnics 2015;66:142–57.
Gui Y, Zhao GF. Modelling of laboratory soil desiccation cracking using DLSM with a two-phase bond model. Computers and Geotechnics 2015;69:578–87.
Gui YL, Bui HH, Kodikara J, Zhang QB, Zhao J, Rabczuk T. Modelling the dynamic failure of brittle rocks using a hybrid continuum-discrete element method with a mixed-mode cohesive fracture model. International Journal of Impact Engineering 2016a;87:146–55.
Gui YL, Zhao ZY, Ji J, Wang XM, Zhou KP, Ma SQ. The grain effect of intact rock modelling using discrete element method with Voronoi grains. Géotechnique Letters 2016b;6(2):136–43.
Gui YL, Zhao ZY, Zhang C, Ma SQ. Numerical investigation of the opening effect on the mechanical behaviours in rocks under uniaxial loading using hybrid continuum-discrete element method. Computers and Geotechnics 2017;90:55–72.
Haeri H, Shahriar K, Marji MF, Moarefvand P. Experimental and numerical study of crack propagation and coalescence in pre-cracked rock-like disks. International Journal of Rock Mechanics and Mining Sciences 2014;67:20–8.
Hoek E, Kaiser PK, Bawden WF. Support of underground excavations in hard rock. Rotterdam, the Netherlands: A.A. Balkema; 1995.
Hoek E, Carranza-Torres CT, Corkum B. Hoek-Brown failure criterion - 2002 edition. In: Hammah R, Bawden W, Curran J, Telesnicki M, editors. Proceedings of the 5th north American rock mechanics Symposium (NARMS-TAC). Toronto, Canada: University of Toronto Press; 2002. p. 267–73.
Itasca. UDEC manual. Minneapolis, USA: Itasca Consulting Group, Inc.; 2008.
Jaeger JC, Cook NGW, Zimmerman RW. Fundamentals of rock mechanics. 4th ed. Blackwell Publishing Ltd.; 2007.
Lin P, Wong RHC, Tang CA. Experimental study of coalescence mechanisms and failure under uniaxial compression of granite containing multipore holes. International Journal of Rock Mechanics and Mining Sciences 2015;77:313–27.
Marinos V, Marinos P, Hoek E. The geological strength index: applications and limitations. Bulletin of Engineering Geology and the Environment 2005;64(1):55–65.
Masoudian MS, Hashemi MA. Analytical solution of a circular opening in an axisymmetric elastic-brittle-plastic swelling rock. Journal of Natural Gas Science and Engineering 2016;35:483–96.
Masoudian MS, Hashemi MA, Tasalloti A, Marshall AM. Elastic-brittle-plastic behaviour of shale reservoirs and its implications on fracture permeability variation: an analytical approach. Rock Mechanics and Rock Engineering 2018;51:1565–82.
Peng J, Wong LNY, Teh CI, Li ZH. Modelling micro-cracking behaviour of Bukit Timah granite using grain-based model. Rock Mechanics and Rock Engineering 2018;51(1):135–54.
Potyondy DO, Cundall PA. A bonded-particle model for rock. International Journal of Rock Mechanics and Mining Sciences 2004;41(8):1329–64.
Sammis CG, Ashby MF. The failure of brittle porous solids under compressive stress states. Acta Metallurgica 1986;34(3):511–26.
Wong RHC, Lin P, Tang CA. Experimental and numerical study of splitting failure of brittle solids containing single pore under uniaxial compression. Mechanics of Materials 2006;38(1–2):142–59.
Yang SQ, Huang YH, Jing HW, Liu XR. Discrete element modelling on fracture coalescence behaviour of red sandstone containing two unparallel fissures under uniaxial compression. Engineering Geology 2014;178:28–48.
Yang SQ, Ranjith PG, Gui YL. Experimental study of mechanical behaviour and X-ray micro CT observation of sandstone under conventional triaxial compression. Geotechnical Testing Journal 2015a;38(2):179–97.
Yang SQ, Xu T, He L, Jing HW, Wen S, Yu QL. Numerical study on failure behaviour of brittle rock specimen containing pre-existing combined flaws under different confining pressure. Archives of Civil and Mechanical Engineering 2015b;15(4):1085–97.

Junlong Shang is a research fellow of Civil and Environmental Engineering at Nanyang Technological University (NTU), Singapore. He joined NTU from the University of Leeds, where he was a postgraduate researcher. He received his PhD in earth sciences from the University of Leeds in 2016 and Bachelor's degree in mining engineering from Central South University (CSU) in 2010. Dr. Shang's main research interests involve experimental rock mechanics, discrete element modelling (DEM), and geothermal energy. Dr. Shang has received several awards, including the distinguished Master thesis award (granted by Hunan Province, China in 2015) and top-10 Master student award (ranking the 1st, granted by CSU in 2012). His PhD thesis was nominated for the 2020 Rocha Medal of the International Society for Rock Mechanics and Rock Engineering (ISRM). Dr. Shang serves as reviewer for around 10 international journals in his field, and external reviewer for the 2019 National Fund for Scientific and Technological Development (Chile). He served as an organising committee member for the 10th Asian Rock Mechanics Symposium (ARMS 10), Singapore, and chair for two technical sessions. Dr. Shang has published 20 SCI journal papers in the field of rock mechanics and rock engineering, and he is the first/corresponding author of 16 JCR Q1 journal papers, one of which published in *Engineering Geology* has been selected as ESI highly cited paper in 2018.